Detailed Electromagnetic Transient Model of Switched Reluctance Motor Drive System

Seyedarmin Mirnikjoo, Mohammed Naidjate, Jean Mahseredjian, Nicolas Bracikowski and Paul Akiki

***Abstract*--This paper focuses on the electromagnetic transient modeling of the switched reluctance motor drive system through the detailed circuit-based representation of the machine, power converter and control system. The dynamic model of the switched reluctance machine consists of interconnected mechanical, electrical and magnetic equivalent circuits in simultaneous solution. The mesh-based permeance network is used to model the nonlinear magnetic behavior of the rotor and stator while the airgap is modeled with variable permeances, enabling transient studies without re-meshing or reconnecting nodes during runtime. The accuracy of the proposed model is validated through comparison with a finite element-based model, demonstrating its reliability while offering significantly faster computational performance. The proposed model simulates the complete switched reluctance drive system under transient conditions.**

***Keywords*: switched reluctance motor, drive system, permeance network, airgap permeance, mechanical dynamics.**

I. Introduction

SWITCHED reluctance motor (SRM) drive system is used in various applications such as pumps, household appliances and electric vehicles [1], [2]. Several models have been developed to represent the electromagnetic behavior of SRM drive systems. However, achieving an accurate and computationally efficient SRM model that can seamlessly be integrated with the drive system and external circuits remains a challenge.

The magnetic behavior of SRMs is highly nonlinear since they mostly operate in magnetic saturated regions to enhance torque production. Additionally, the significant fringing and leakage flux of SRMs, caused by their large slot openings, are not negligible [3], [4]. Therefore, accurate incorporation of the nonlinear and complex magnetic behavior of SRMs is essential for achieving correct and acceptable results [5]. In fact, the development of detailed models using magnetic circuits is a first step in the development of typical lumped circuit models used in EMT-type software.

The finite element method (FEM) accurately models the nonlinear magnetic behavior of the SRM, but it is computationally very expensive [6], [7]. Additionally, commercial FEM packages lack power and control components. In this regard, the co-simulation of FEM packages and circuit simulators facilitates the integration of the SRM's FEM model into its drive system model [8]. However, this indirect coupling requires multiple iterations between field and circuit equations, leading to high computational burden and numerical delays.

In many articles, the nonlinear magnetic characteristics of SRM such as inductance, flux linkage and torque are integrated into its drive system model through curve-fitting techniques [9], Fourier series [10], [11] or lookup tables (LUTs) generated from magnetostatic FEM [12], [13]. However, these methods are not generic as they require rerunning magnetostatic FEM to regenerate new LUTs or calculate new coefficients in curve-fitting or Fourier series techniques. Moreover, the machine's internal magnetic behavior, like magnetic flux density distribution, is not accessible in these methods.

Circuit-based modeling of electromagnetic devices enables seamless and simultaneous-solution integration of these devices within large external circuits since these models can be implemented in circuit-based software like EMTP® [14] which offers an extensive library of components, ranging from transmission lines to power electronics devices and control diagram blocks. In [15]-[17], a circuit-based approach known as the permeance network method (PNM) is employed to model the inductor and transformer in EMTP®. This model benefits from simultaneous solutions of magnetic and electrical circuits while considering geometric characteristics and nonlinear magnetic behavior of the electromagnetic device.

The PNM is widely used for modeling the nonlinear magnetic behavior of SRMs where the main challenge lies in modeling the SRM rotation [18]. In [19], a flux-tube-based approach is used to generate the permeance network within stator, rotor and airgap. However, this method requires predefining the flux paths within various parts of the machine. Although implementing a mesh-based permeance network could satisfy the generic aspects and improve the model accuracy [20], [21], using the mesh-based approach within airgap cannot model the SRM rotation in a computationally efficient way. The circuit nodes at the airgap boundary should be reconnected at each time-step while the machine is rotating at a fixed speed. Also, in transient studies, dynamic and unpredictable variations of machine speed necessitate

Seyedarmin Mirnikjoo is with the department of Electrical Engineering, Polytechnique Montreal, H3T 1J4 Montreal, QC, Canada (seyedarmin.mirnikjoo@polymtl.ca)
Mohammed Naidjate is with the department of Electrical Engineering, Polytechnique Montreal, H3T 1J4 Montreal, QC, Canada (mohammed.Naidjate@polymtl.ca)
Jean Mahseredjian is with the department of Electrical Engineering, Polytechnique Montreal, H3T 1J4 Montreal, QC, Canada (jean.mahseredjian@polymtl.ca)
Nicolas Bracikowski is with the IREENA Laboratory of Nantes University, 44600 Saint-Nazaire, France. (nicolas.bracikowski@univ-nantes.fr)
Paul Akiki is with the EDF-R&D, Électricité de France, 91120 Palaiseau, France (paul.akiki@edf.fr)

Paper submitted to the International Conference on Power Systems Transients (IPST2025) in Guadalajara, Mexico, June 8-12, 2025.

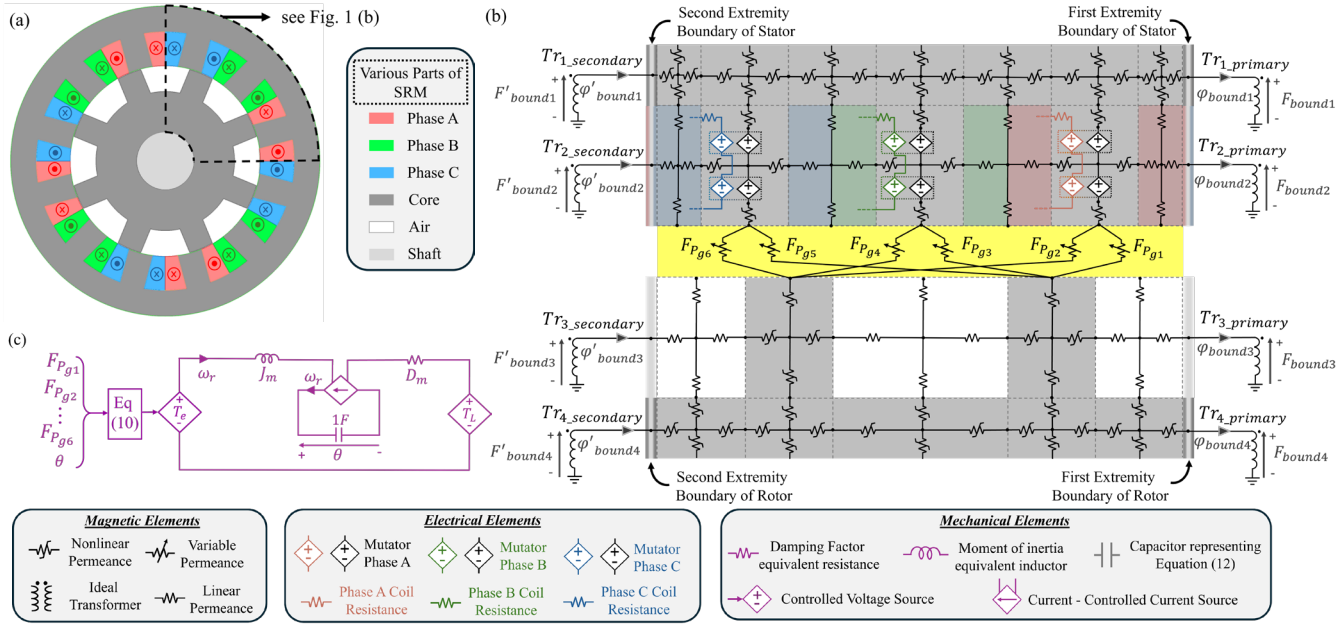

Fig. 1: SRM and its detailed dynamic model, (a) the geometry of a 3-phase 12/8 SRM, (b) the permeance network coupled with the electric circuit, (c) the mechanical equivalent circuit

remeshing and regenerating the permeance network at each time-step. Additionally, the mesh-based airgap approach requires a high number of mesh elements in the airgap part to reach an acceptable model accuracy. Using a high number of mesh elements in the airgap increases the computational burden, making the mesh-based airgap model inefficient for studies focusing on the transient behavior of the whole drive system. Also, the necessity of using small simulation time-steps because of the presence of the power electronics devices in these transient studies further limits the practicality of meshed airgap approaches in electromagnetic transient (EMT) studies.

These challenges are addressed by using a mesh-free airgap permeance method that allows random rotation angles and maintains the same circuit topology during simulation. Analytical functions [22] or FEM-based calculations [23] can estimate the airgap permeance values. However, using FEM-based calculations requires rerunning FEM simulations as preprocessing whenever machine geometrical parameters change.

This paper presents a new efficient and detailed EMT (DEMT) model of the SRM drive system. Each component of the SRM drive system including the power converter, controller and machine is modeled in detail by circuit-based representation and with a simultaneous solution with the drive system's components. The dynamic model of the SRM consists of three equivalent circuits representing the magnetic, electrical and mechanical interactions of SRM by a simultaneous solution.

The results of the proposed DEMT model of the SRM drive system are verified by those obtained from the FEM-based one. Moreover, the proposed DEMT model is used to model the electromagnetic transient behavior of the SRM drive system under various operating conditions.

This paper is organized as follows. The new detailed dynamic model of the SRM is presented in section II. In section III, the DEMT model of the SRM drive system is developed by integrating the SRM's detailed dynamic model into the circuit-based EMT model of the power converter and its controller. Section IV presents the verification of the proposed DEMT model and the results obtained from transient studies conducted with the proposed DEMT model.

II. Detailed Dynamic Model of SRM

The detailed dynamic model of the SRM consists of three interconnected circuits representing the electrical, magnetic, and mechanical behavior of SRM with a simultaneous solution between these circuits, as shown in Fig. 1. The geometry of a 3-phase SRM with 12 stator poles and 8 rotor teeth, named 12/8 SRM is shown in Fig. 1 (a). In this study, a quarter of this machine is modeled due to the symmetry. In this regard, the interconnected permeance network and electrical circuit of a quarter of this machine is shown in Fig. 1 (b). In this figure, the magnetic circuit is colored in black. Also, the equivalent circuit of SRM's mechanical dynamic is shown in Fig. 1 (c) (in purple).

A. Magnetic Circuit

The magnetic behavior of SRM is modeled by the PNM. As shown in Fig. 1 (b), the permeance network of the rotor and stator is built by a mesh-based approach while they are connected through variable permeances of airgap.

1) Permeance network of the rotor and stator

As shown in Fig. 1 (b), the teeth and slots of the rotor and stator are subdivided into several elements. The number of mesh elements in the radial direction can be selected based on the required model accuracy. The effect of the number of mesh elements on the model's accuracy and computational time is studied in section IV. The radial and orthoradial directions of the flux path within mesh elements are modeled by four permeances perpendicularly connected at the element centroid.

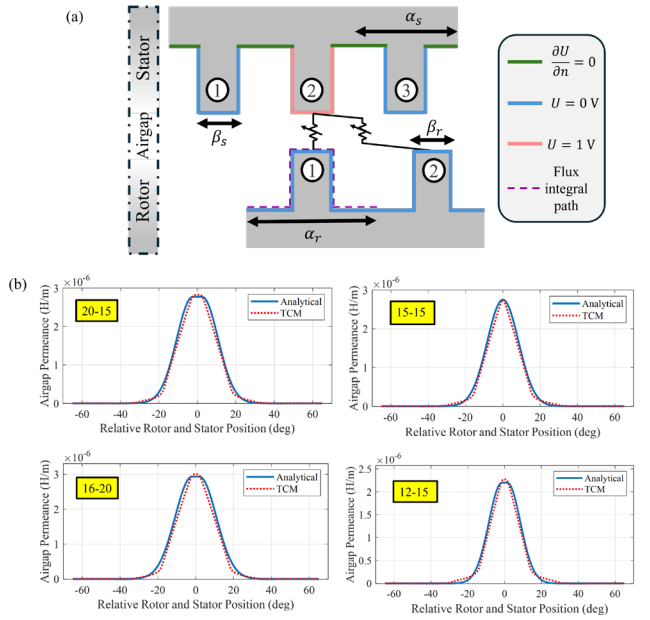

Fig. 2: Airgap permeance values for different rotor and stator teeth angles calculated by TCM and analytical function

Due to the constant permeability of the rotor and stator slots, the mesh elements associated with slots consist of linear permeances. Values of these linear permeances correspond to the radial and orthoradial equivalent permeances of a cylindrical shape flux tube. Further details regarding cylindrical shape flux tubes are available in [24] and [25]. Moreover, the nonlinear permeances represent the nonlinear magnetic behavior of the ferromagnetic core in mesh elements related to the stator and rotor teeth and yokes. These nonlinear permeances are implemented by their Norton companion models, whose details are presented in [26], [27].

2) Mesh-free model of the airgap

As depicted in Fig. 1 (b), each node on the stator tooth-airgap boundary (nodes of stator teeth at the top of the yellow part in Fig. 1 (b)) is connected to all nodes on the rotor tooth-airgap boundary (nodes of rotor teeth at the bottom of the yellow part in Fig. 1 (b)) through variable permeances. The value of the airgap variable permeance changes according to the rotor position to accommodate rotation. In this regard, correct estimation of the airgap permeance values in various rotor positions is crucial for reaching an acceptable accuracy of the SRM's magnetic model. Thus, the value of the airgap permeance is derived from the tooth contour method (TCM) [28], [29]. Fig. 2 (a) shows the imposed boundary condition in TCM. As shown in this figure, TCM calculates the value of the airgap permeance based on the difference in magnetic potential (U in Fig. 2 (a)) between a stator tooth edge and the other teeth. The magnetic flux passing through the selected rotor tooth, resulting from the magnetic potential difference, is estimated by using FEM for various rotor positions. Thus, the airgap permeance value can be estimated as

$$P_{g_{i,j}}(\theta) = \frac{\varphi_j(\theta)}{\Delta U_{i,j}} \tag{1}$$

where $P_{g_{i,j}}$ is the value of the airgap permeance connecting the tooth i of the stator to the tooth j of the rotor, θ is the rotor position, φ_j represents the flux passing through the tooth j of the rotor, and $\Delta U_{i,j}$ is the magnetic potential difference between the tooth i of the stator and the tooth j of the rotor.

Although the TCM benefits from accuracy, it requires long preparation time and necessitates running FEM simulations as preprocessing. Another drawback of this method is the need for interpolation between precalculated values at each time-step. To tackle the mentioned problems, this article employs an efficient analytical method that is easy to configure. The TCM is used for verification of the proposed analytical method. In the proposed analytical method, the relative position of the stator and rotor teeth are categorized as fully overlapped regions (like the relative position of tooth 1 of the rotor and tooth 2 of the stator in Fig. 2 (a)), partially overlapped (like the relative position of tooth 2 of the rotor and tooth 3 of the stator in Fig. 2 (a)), and null overlapped (like the relative position of rotor tooth 2 and tooth 1 of the stator in Fig. 2 (a)). The value of the airgap permeance is assumed to be constant in the fully overlapped region [30]. Also, it has been concluded that an exponential function can model the value of the airgap permeance in partially and null overlapped regions with acceptable accuracy [31]. Hence, an exponential function is adapted in this study to estimate airgap permeances in partially and null overlapped regions. The functions describing the airgap permeance values are:

$$P_{g_{i,j}} = \begin{cases} P_{g_m} & \theta_{i,j} \le \beta_{m_{i,j}} \\ P_{g_m} \exp\left(-\left[\dfrac{\theta_{i,j} - \beta_{m_{i,j}}}{\beta_{Z_{i,j}} - \beta_{m_{i,j}}} \right]^2 \right) & \theta_{i,j} > \beta_{m_{i,j}} \end{cases} \tag{2}$$

$$\theta_{i,j} = \theta + \sigma_{i,j} \tag{3}$$

$$\beta_{m_{i,j}} = \frac{\left| \beta_{s_i} - \beta_{r_j} \right|}{2} \tag{4}$$

$$\beta_{Z_{i,j}} = \frac{\alpha_s}{\alpha_r} \frac{\left| \beta_{s_i} + \beta_{r_j} \right|}{2} \tag{5}$$

where β_{s_i} is the angle of the tooth i of the stator, β_{r_j} is the angle of the tooth j of the rotor, $\sigma_{i,j}$ is the relative position between tooth i of the stator and tooth j of the rotor tooth, α_s is the stator pole pitch, α_r is the rotor pole pitch and P_{g_m} is the maximum value of the airgap permeance. Fig. 2 (b) compares airgap permeance values calculated by the TCM and the proposed analytical function, for various stator and rotor teeth angle combinations. In this figure, the stator and rotor teeth angle are shown in the yellow box. As can be seen, the proposed analytical function can model airgap permeance with acceptable accuracy for fully, partially, and non-overlapped relative positions of the stator and rotor teeth.

3) Antiperiodic boundary condition

As shown in Fig. 1 (a) and Fig. 1 (b), the domain of study is reduced to a quarter of the machine due to the machine's geometrical symmetry. Based on the winding pattern of the 12/8 SRM shown in Fig. 1 (a), the antiperiodic boundary condition should be imposed in the permeance network. In the antiperiodic boundary condition, the nodes on the two extremity boundaries of the domain (shown in Fig. 1 (b)) should be connected in a way that satisfies the following equations [29]

$$F'_{bound} = -F_{bound} \tag{6}$$

$$\varphi'_{bound} = -\varphi_{bound} \tag{7}$$

where F_{bound} is the magnetic potential of the nodes on the first boundary, F'_{bound} represents the magnetic potential of the nodes on the second boundary, φ_{bound} is the flux passing through the nodes on the first boundary, and φ'_{bound} is the flux passing through the nodes on the second boundary. In this regard, the ideal transformers with a transformation ratio of -1 are used to implement the antiperiodic boundary condition in the circuit-based model, as shown in Fig. 1 (b). As shown in this figure, these transformers' primaries ($T_{r\_primary}$ in Fig. 1 (b)) and secondaries ($T_{r\_secondary}$ in Fig. 1 (b)) are connected to the nodes on the first and second boundaries.

B. Electric Circuit

According to Faraday's law, the electrical and magnetic circuits are strongly coupled through mutators. Mutators transfer the electrical current into the magnetic circuit as a source of magnetomotive force (MMF) and convert the flux of the magnetic circuit into the electrical circuit as a source of electromotive force (EMF). Thus, the MMF and EMF of the mutator can be calculated as [32]

$$F = Ni \tag{8}$$

$$e = -N\frac{d\varphi}{dt} \tag{9}$$

where F is the MMF of the mutator, e represents the EMF of the mutator, i is the current in the electric circuit, φ is the flux passing through the magnetic circuit and the gain of the mutator is represented by N which can be calculated by applying Ampere's law. Further details regarding mutators and their gain calculation can be found in [15], [16].

C. Mechanical Circuit

The electromagnetic torque of the SRM can be calculated based on co-energy [33]

$$T_e = \sum_{n=1}^{n_g} \frac{\partial P_{g_n}}{\partial \theta} \frac{{F_{P_{g_n}}}^2}{2} \tag{10}$$

where T_e represents the electromagnetic torque, n_g is the total number of airgap variable permeances (6 in Fig. 1 (b)) and F_{P_g} is the MMF of each airgap permeance. The mechanical equations of the machine are written as [34]

$$T_e - T_L = J_m\frac{d\omega_r}{dt} + D_m\omega_r \tag{11}$$

$$\omega_r = \frac{d\theta}{dt} \tag{12}$$

where the load torque is represented by T_L, J_m is the moment of inertia, D_m is the damping factor and the machine speed is expressed as ω_r. Therefore, the circuit-based representation of the machine's mechanical equations is depicted in Fig. 1 (c) (the purple circuit) and enables the simultaneous solution of mechanical equations with corresponding magnetic and electrical circuits.

III. DEMT Model of SRM Drive System

The schematic diagram of the SRM drive system components is shown in Fig. 3. This figure shows that an asymmetric bridge converter supplies the SRM while allowing for independent control of phase currents. Each phase of the asymmetric bridge converter consists of two IGBTs and two diodes. This study implements the detailed circuit-based model for IGBTs and diodes. Further details regarding the detailed circuit-based representation of the power electronic components for EMT studies are available in [35].

Moreover, the control system consists of speed, current and position control schemes [36], which are interdependent, as shown in Fig. 3. The sequential excitation of SRM phase windings is enabled by the position control. The conduction angle of each phase at each electric cycle θ_{cond} is the difference between the turn-on angle θ_{on} and turn-off angle θ_{off} as

$$\theta_{cond} = \theta_{off} - \theta_{on} \tag{13}$$

The pulse widths of phases (S_{pos_a}, S_{pos_b}, and S_{pos_c} in Fig. 3) at each electric cycle are equal to θ_{cond} while there is a 120-degree phase shift between phases. Additionally, the hysteresis current control is implemented to maintain the SRM phase current at the reference current I_{ref}. The value of the reference current I_{ref} at each time-step is determined by the speed controller based on the machine's speed and speed command, as illustrated in Fig. 3. The DEMT model of the SRM drive system is built by integration of the detailed dynamic model of the SRM proposed in section II into the detailed circuit-based EMT model of the asymmetric bridge and the control system. The DEMT model benefits from the simultaneous solutions between all components of the SRM drive system.

IV. Results and Verification

In this section, a 3-phase 12/8 SRM and its drive system are selected as a case study. The geometric specification of the studied SRM is available in [21] (refer to 12/8 in TABLE I in [21]). The specification of the drive system and mechanical parameters of the SRM are presented in TABLE I. This model is implemented in the circuit-based EMT simulation engine EMT-Julia, which the authors developed under the Julia environment. EMT-Julia uses the same methodology as

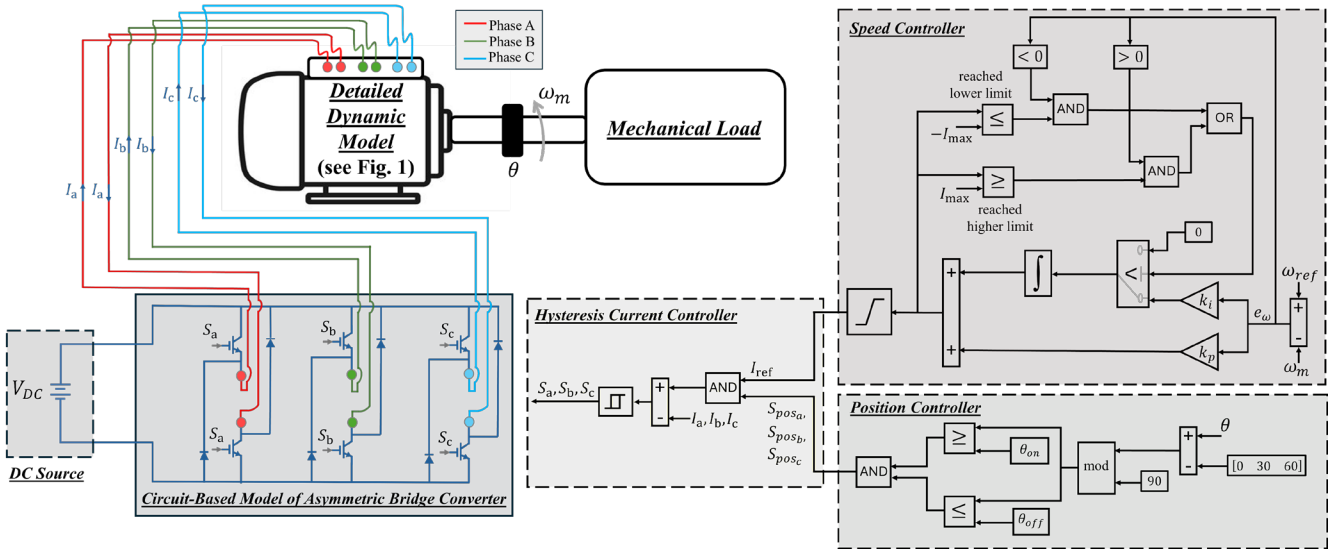

Fig. 3: DEMT model of the SRM drive system

TABLE I:
Studied SRM Drive System Specification and its Mechanical Parameter

Parameter	Symbol	Value
Turn ON angle	θ_{on}	0 [deg]
Turn OFF angle	θ_{off}	22.5 [deg]
Stator tooth angle	θ_{ts}	15 [deg]
Rotor tooth angle	θ_{tr}	15 [deg]
DC link voltage	V_{DC}	300 [V]
Phase coil resistance	R_{ph}	0.21 [Ω]
Stack length	L_{stk}	70 [mm]
Stator outer diameter	D_o	136 [mm]
Damping coefficient	D_m	0.000608 [Nm.s/rad]
Rotor moment of inertia	J_m	0.0003318 [Kg.m^2]

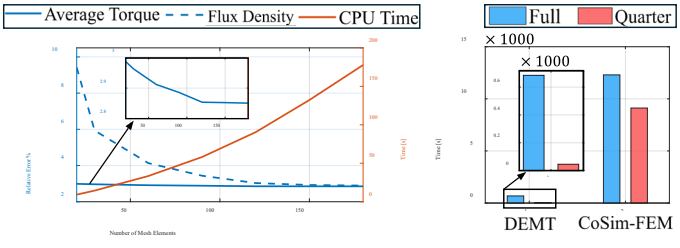

(a) (b)

Fig. 4: Accuracy and computational time evaluation of DEMT, (a) effect of mesh elements number, (b) effect of using symmetry

EMTP®. Components exhibiting dynamic behavior can be discretized using trapezoidal integration or backward Euler. In this study, we used trapezoidal integration. The matrix system is constructed based on the modified augmented nodal analysis (MANA) method [14] and solved by the KLU solver.

A. DEMT Verification

To validate DEMT's performance, the results of DEMT are compared with those obtained from the FEM-based model. This FEM-based model is developed by implementing the FEM model of the studied SRM in ANSYS Maxwell® while the FEM model of SRM is integrated with the asymmetric bridge converter and controller model in Simplorer® through co-simulation. This model is named CoSim-FEM in this article. Both DEMT and CoSim-FEM were simulated on a 2.5 GHz, Core i7-11850H computer with 64 GB of RAM.

The first step in implementing DEMT is to determine the optimal number of mesh elements that balances the required accuracy with computational time. Thus, the average torque value and the magnetic flux density at the center of the stator tooth aligned with the rotor tooth serve as the metrics for the mesh assessment. Fig. 4 (a) shows the effect of mesh element numbers on the computational time and relative error of the selected metrics. In this assessment, SRM rotates at a fixed speed for 12 ms, using a time step of 1 µs while a quarter of the machine is modeled. As shown in Fig. 4 (a), increasing the number of mesh elements reduces the relative error of both average value of the torque and magnetic flux density, but significantly increases computational time. Thus, based on the required computational speed and accuracy in this study, 72 mesh elements are used in the following analysis.

Moreover, Fig. 4 (b) shows the effect of using symmetry (modeling a quarter of the machine) on the computational time of the proposed DEMT and CoSim-FEM. Comparing the simulation time for the proposed DEMT illustrates that in this study modeling a quarter of machine speeds up the simulation process by more than 14 times compared to modeling the full geometry of the machine. In case of CoSim-FEM, modeling a quarter of the machine reduced the CPU time from 3h 25min (the CPU time of CoSim-FEM with full geometry model of SRM) to 2h 32min. Therefore, modeling a quarter of machine considerably accelerates the DEMT simulation process compared to the CoSim-FEM. The lesser acceleration in simulation process of CoSim-FEM is due to the added computational burden of remeshing FEM model at each time-step and co-simulation. In contrast, DEMT not only benefits from a simultaneous solution of the drive system components but also uses the same magnetic circuit topology throughout the entire simulation, thanks to the mesh-free techniques in the airgap.

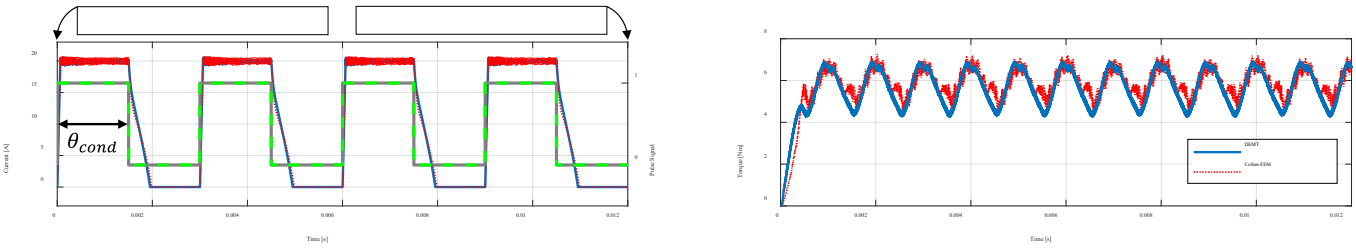

(a) (b)

Fig. 5: SRM outputs while SRM rotates at 2500 rpm, (a) phase current, (b) electromagnetic torque

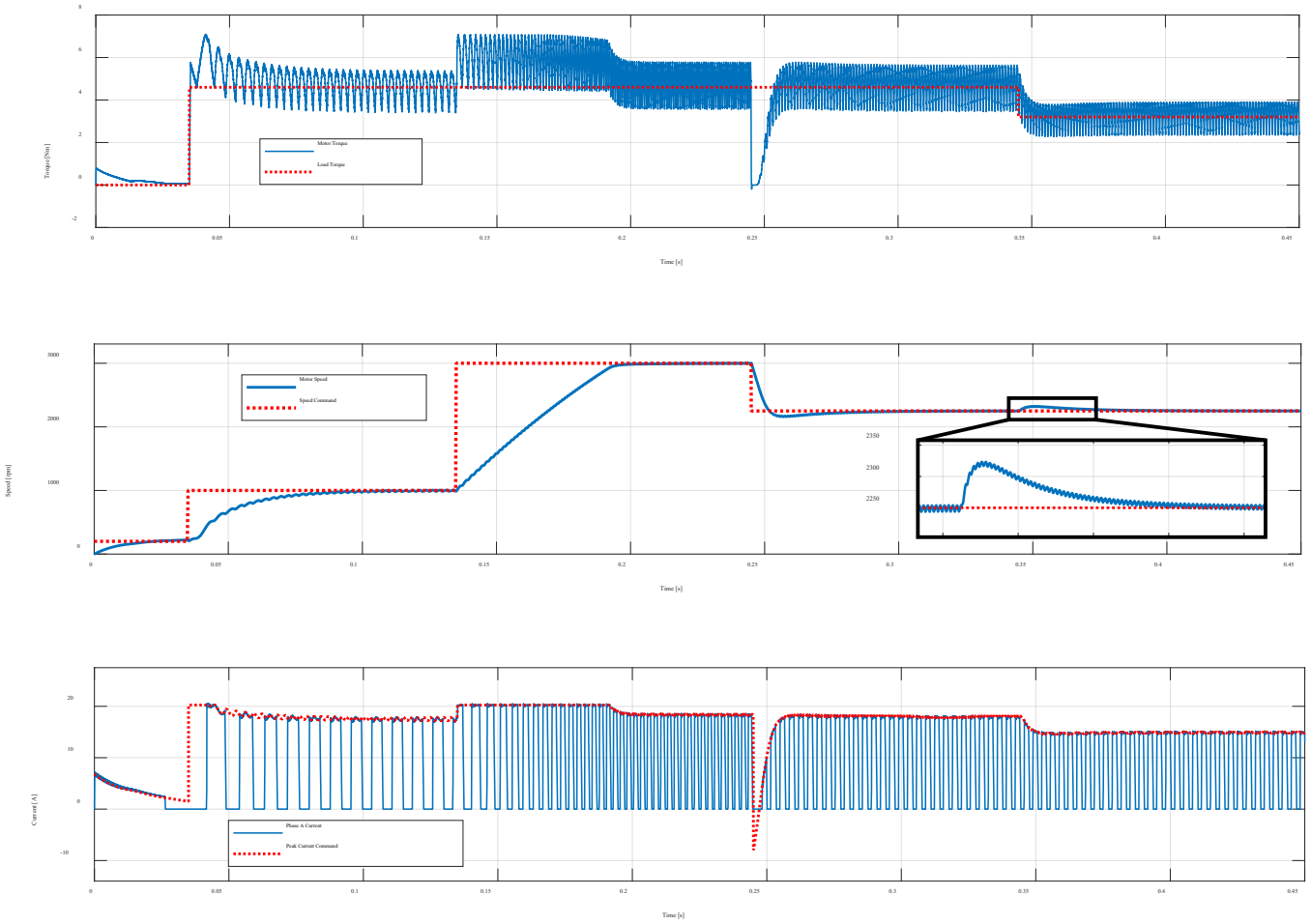

Fig. 6: Transient output characteristics of the SRM drive system due to the sudden changes in the load torques and speed commands, (a) torque, (b) motor speed and speed commands, and (c) current of phase A and the command of phase peak

Furthermore, the studied SRM motor drive system is simulated with DEMT and CoSim-FEM when the machine is rotating at a fixed speed of 2500 rpm while the hysteresis current control maintains the phase current in 20 A. The phase current of the studied SRM is presented in Fig. 5 (a). The phase currents calculated by DEMT and CoSim-FEM show good agreement. In both models, the phase current is tracking the related control commands (phase pulses) whereas both models exhibit a tracking error at the turn-off angle due to the inductive nature of the SRM. It is worth mentioning that the currents of phases B and C are similar to the current of phase A with 120 and 240 electrical phase shifts.

Fig. 5 (b) compares the SRM torque calculated by DEMT and CoSim-FEM, showing that DEMT provides acceptable accuracy. CoSim-FEM exhibits more high frequency oscillations in the torque, likely due to its higher number of mesh elements and numerical oscillations from remeshing.

B. Transient study: Sudden variations in load torque and speed

In this section, the transient behavior of the SRM drive system is studied. Fig. 6 presents the transient output characteristics of the studied SRM drive system while there are sudden changes in load and speed. As shown in Fig. 6 (a), the machine starts to work in the no-load condition ($T_L = 0$ Nm) while the speed command is equal to 200 rpm (see Fig. 6 (b)). At $t = 0.035$ s, the mechanical load T_L of 4.6 Nm is applied

and the speed command is increased to 1000 rpm. The machine experienced a transient and reached the steady-state below $t =$ 0.1 s. At $t = 0.135$ s, the speed command is suddenly increased from 1000 rpm to 3000 rpm while the load torque remains at 4.6 Nm. The machine accelerates until it reaches the steady-state at about $t = 0.2$ s. At $t = 0.245$ s, the speed command is suddenly reduced from 3000 rpm to 2250 rpm. Finally, the load torque T_L experiences a sudden decrease to 3.4 Nm at $t =$ 0.345 s, while the speed command remains at 2250 rpm. Due to this sudden reduction in the load torque, the motor accelerates before the speed controller regulates the peak phase current to restore the motor speed to 2250 rpm. The values of I_{ref} and phase A current are shown in Fig. 6 (c). It is worth mentioning that the currents of phases B and C are similar to the current of phase A with 120 and 240 degrees phase shifts, respectively.

V. Conclusion

In this paper, the dynamic model of the SRM is developed by interconnecting the equivalent circuits representing the machine's magnetic, electrical and mechanical behavior within a simultaneous solution. The mesh-based permeance network is used to model the nonlinear magnetic behavior of the rotor and stator. Thus, the proposed permeance network is fully parametrized and can automatically adapt to changes in the machine's geometry while it allows a trade-off between computation time and model accuracy. To model the machine's rotation without changing the magnetic circuit topology, the airgap part is modeled by the mesh-free approach through variable permeances.

The new DEMT model of the SRM drive system is developed by seamlessly integrating the proposed dynamic model of SRM into the detailed circuit-based model of the power converter and its related control system. This model benefits from a simultaneous solution between the machine and drive system components. Comparing the proposed DEMT model with the FEM-based model verifies its accuracy and shows its significantly lower computational burden. Furthermore, the proposed DEMT model simulates the transient behavior of the SRM drive system under various loads.

VI. References

[1] R. Rocca, G. De Donato, P. Bolognesi, C. Boccaletti, and F. G. Capponi, "Improved Design-Oriented Analytical Modelling of Switched Reluctance Machines Based on Fröhlich-Kennelly Equations," *IEEE Transactions on Energy Conversion,* 2023.

[2] S. Song, J. Zhong, C. Yang, C. Bao, L. Ge, Z. Fu, R. Ma, and W. Liu, "Smooth Low-Speed Sensorless Control of Switched Reluctance Machine With Heavy Load," *IEEE Transactions on Industrial Electronics,* vol. 71, no. 4, pp. 3361-3370, 2024.

[3] B. Bilgin, J. W. Jiang, and A. Emadi, *"Switched reluctance motor drives: fundamentals to applications"* Boca Raton, FL, 2018.

[4] F. P. Scalcon, G. Fang, C. J. Volpato Filho, H. A. Gründling, R. P. Vieira, and B. Nahid-Mobarakeh, "A review on switched reluctance generators in wind power applications: Fundamentals, control and future trends," *IEEE Access,* vol. 10, pp. 69412-69427, 2022.

[5] F. Soares and P. C. Branco, "Simulation of a 6/4 switched reluctance motor based on Matlab/Simulink environment," *IEEE transactions on aerospace and electronic systems,* vol. 37, no. 3, pp. 989-1009, 2001.

[6] G. Watthewaduge, E. Sayed, A. Emadi, and B. Bilgin, "Electromagnetic modeling techniques for switched reluctance machines: State-of-the-art review," *IEEE Open Journal of the Industrial Electronics Society*, vol. 1, pp. 218-234, 2020.

[7] S. Mohammadi, J. L. Kirtley, and J. H. Lang, "Modeling of a Rotary Actuator Using Elliptical Coordinates and Differential Flux Tubes," *IEEE Transactions on Magnetics*, vol. 59, no. 2, pp. 1-14, 2022.

[8] X. Ling, B. Li, L. Gong, Y. Huang, and C. Liu, "Simulation of switched reluctance motor drive system based on multi-physics modeling method," *IEEE Access*, vol. 5, pp. 26184-26189, 2017.

[9] O. Safdarzadeh, A. Mahmoudi, E. Afjei, and H. Torkaman, "Rotary-linear switched reluctance motor: Analytical and finite-element modeling," *IEEE Transactions on Magnetics*, vol. 55, no. 5, pp. 1-10, 2019.

[10] S. Song, M. Zhang, and L. Ge, "A new decoupled analytical modeling method for switched reluctance machine," *IEEE Transactions on Magnetics*, vol. 51, no. 3, pp. 1-4, 2015.

[11] F. R. Salmasi and B. Fahimi, "Modeling switched-reluctance machines by decomposition of double magnetic saliencies," *IEEE Transactions on Magnetics*, vol. 40, no. 3, pp. 1556-1561, 2004.

[12] Z. Wang, X. Cao, Z. Deng, and J. Cai, "Electromagnetic modeling and investigation for bearingless switched reluctance motor considering magnetic saturation," *IEEE Transactions on energy conversion*, vol. 38, no. 1, pp. 122-133, 2022.

[13] J. Dong, B. Howey, B. Danen, J. Lin, J. W. Jiang, B. Bilgin, and A. Emadi, "Advanced dynamic modeling of three-phase mutually coupled switched reluctance machine," *IEEE Transactions on Energy Conversion*, vol. 33, no. 1, pp. 146-154, 2017.

[14] J. Mahseredjian, S. Dennetière, L. Dubé, B. Khodabakhchian, L. Gérin-Lajoie, "On a new approach for the simulation of transients in power systems". *Electric Power Systems Research*, Vol. 77, Issue 11, September 2007, pp. 1514-1520.

[15] S. R. Pordanjani, J. Mahseredjian, M. Naïdjate, N. Bracikowski, M. Fratila, and A. Rezaei-Zare, "Electromagnetic modeling of inductors in EMT-type software by three circuit-based methods," *Electric Power Systems Research*, vol. 211, p. 108304, 2022.

[16] S. R. Pordanjani, M. Naïdjate, N. Bracikowski, M. Fratila, J. Mahseredjian, and A. Rezaei-Zare, "Electromagnetic Modeling of Transformers in EMT-Type Software by a Circuit-Based Method," *IEEE Transactions on Power Delivery*, vol. 37, no. 6, pp. 5402-5413, 2022.

[17] J. Mahseredjian, M. Naidjate, M. Ouafi, and J. A. O. Wilches, "Electromagnetic Transients Simulation Program: A unified simulation environment for power system engineers," *IEEE Electrification Magazine*, vol. 11, no. 4, pp. 69-78, 2023.

[18] F. E. Fleming and C. S. Edrington, "Real-time emulation of switched reluctance machines via magnetic equivalent circuits," *IEEE Transactions on Industrial Electronics*, vol. 63, no. 6, pp. 3366-3376, 2016.

[19] G. Davarpanah and J. Faiz, "Nonlinear modeling of a C-core connected two-phase switched reluctance motor," *IEEE Transactions on Energy Conversion,* vol. 36, no. 4, pp. 2761-2769, 2021.

[20] G. Watthewaduge and B. Bilgin, "Radial force density calculation of switched reluctance machines using reluctance mesh-based magnetic equivalent circuit," *IEEE Open Journal of the Industrial Electronics Society*, vol. 3, pp. 37-49, 2021

[21] G. Watthewaduge and B. Bilgin, "Reluctance mesh-based magnetic equivalent circuit modeling of switched reluctance motors for static and dynamic analysis," *IEEE Transactions on Transportation Electrification*, vol. 8, no. 2, pp. 2164-2176, 2021.

[22] X. Sun, K. Diao, G. Lei, Y. Guo, and J. Zhu, "Real-time HIL emulation for a segmented-rotor switched reluctance motor using a new magnetic equivalent circuit," *IEEE Transactions on Power Electronics*, vol. 35, no. 4, pp. 3841-3849, 2019

[23] W. Peng and J. Gyselinck, "Combined magnetic-equivalent-circuit and finite-element modelling of switched reluctance machines," in *2016 IEEE International Energy Conference (ENERGYCON)*, 2016: IEEE, pp. 1-6.

[24] A. Beirami, H. F. Farahani, R. M. Rahimi, and S. Amini, "Dynamic analysis of Halbach coaxial magnetic gears based on magnetic equivalent circuit modelling," *IET Circuits, Devices & Systems,* vol. 15, no. 3, pp. 260-271, 2021.

[25] S. Mohammadi and M. Mirsalim, "Double-sided permanent-magnet radial-flux eddy-current couplers: three-dimensional analytical modelling, static and transient study, and sensitivity analysis," *IET Electric Power Applications,* vol. 7, no. 9, pp. 665-679, 2013.

[26] M. Yin, N. Mohammed, N. Bracikowski, A. Pierquin, and D. Trichet, "Topology Optimization of Coaxial Magnetic Gear based on Reluctance

Network Analysis," in *2024 International Conference on Electrical Machines (ICEM)*, 2024: IEEE, pp. 1-8.
[27] M. Yin, M. Naidjate, N. Bracikowski, A. Pierquin, and D. Trichet, "Topology optimization of non-linear electromagnetic actuator based on Reluctance Network Analysis," *Journal of Magnetism and Magnetic Materials,* vol. 602, p. 172174, 2024.
[28] E. Ilhan, J. Paulides, L. Encica, and E. Lomonova, "Tooth contour method implementation for the flux-switching PM machines," in *The XIX International Conference on Electrical Machines-ICEM 2010*, 2010: IEEE, pp. 1-6.
[29] S. Alli, N. Bracikowski, L. Moreau, and M. Zaïm, "Reluctance network modeling of a low speed doubly salient permanent magnet machine," in *IECON 2017-43rd Annual Conference of the IEEE Industrial Electronics Society*, 2017: IEEE, pp. 2138-2143.
[30] V. Ostovic, *Dynamics of saturated electric machines*. Springer Science & Business Media, 2012.
[31] A. M. Silva, C. H. Antunes, A. M. Mendes, and F. J. Ferreira, "Generalized reluctance network framework for fast electromagnetic analysis of radial-flux machines," *IEEE Transactions on Energy Conversion,* vol. 38, no. 1, pp. 310-320, 2022
[32] S. Mohammadi, W. R. Benner, J. L. Kirtley, and J. H. Lang, "An Actuator with Magnetic Restoration, Part I: Electromechanical Model and Identification," *IEEE Transactions on Energy Conversion,* 2024.
[33] S. D. Sudhoff, *Power magnetic devices: a multi-objective design approach*. John Wiley & Sons, 2021.
[34] U. Karaagac, J. Mahseredjian, O. Saad, and S. Dennetière, "Synchronous machine modeling precision and efficiency in electromagnetic transients," *IEEE transactions on power delivery,* vol. 26, no. 2, pp. 1072-1082, 2010.
[35] U. Karaagac, J. Mahseredjian, R. Gagnon, H. Gras, H. Saad, L. Cai, I. Kocar, A. Haddadi, E. Farantatos, S. Bu, K. W. Chan, and L. Wang, "A generic EMT-type model for wind parks with permanent magnet synchronous generator full size converter wind turbines," *IEEE Power and Energy Technology Systems Journal,* vol. 6, no. 3, pp. 131-141, 2019.
[36] R. Krishnan, *Switched reluctance motor drives: modeling, simulation, analysis, design, and applications*. CRC press, 2017.